Journal of Materials Chemistry A

ROYAL SOCIETY OF CHEMISTRY

PAPER

View Article Online
View Journal | View Issue

Cite this: J. Mater. Chem. A, 2020, 8, 20162

Fast and all-weather cleanup of viscous crude-oil spills with $Ti_3C_2T_X$ MXene wrapped sponge†

Cheng Gong,‡[a] Junchao Lao, ‡*[b] Bingyv Wang,[b] Xiaoyan Li,[b] Guojie Li,[bc] Jun Gao,[d] Yizao Wan,[e] Xiaohong Sun, [a] Ruisong Guo*[a] and Jiayan Luo *[b]

Received 2nd July 2020
Accepted 8th September 2020

DOI: 10.1039/d0ta06480g

rsc.li/materials-a

Remediation of crude-oil spills is a global challenge. Conventional sorbents are inefficient for complete remediation due to the high viscosity of crude oil. However, heating crude oil can dramatically reduce viscosity, allowing efficient remediation. In this study, we demonstrate that polyurethane sponge wrapped with $Ti_3C_2T_X$ MXene ($Ti_3C_2T_X$@PU) realizes fast and complete remediation of crude oil with the help of Joule heating or photothermal effects. Due to excellent photothermal properties and metal-like conductivity of $Ti_3C_2T_X$, $Ti_3C_2T_X$@PU can quickly adapt to the various conditions in practical applications with the synergistic effect of solar heating and Joule heating. The excellent heating capacity enables $Ti_3C_2T_X$@PU to absorb more than 40 times its own weight of crude oil in 20 min. This all-weather sorbent design provides a promising solution for the cleanup of viscous crude-oil spills.

1. Introduction

Oil spills from offshore oil exploration and production, natural seeps, tanker accidents and industrial discharge, not only threaten local living beings, but also destroy marine ecosystems.[1–3] To remediate oil-spills, various technologies have been used, such as dispersants, skimmers, hardening agents, *in situ* burning and vacuums.[4–9] Unfortunately, they either have side effects on marine life or fail to clean up oil spills promptly. In addition, dissipation, using hardening agents, or burning the oil at the spill site causes secondary contamination. Skimming and vacuuming rarely clean up the oil thoroughly, as their efficiency may be severely affected by spill sites and weather conditions.

Recently, porous absorbent materials with both hydrophobic and lipophilic characteristics were proposed to remediate oil spills. These aerogels,[10–13] sponges,[14–18] foam[19,20] and membranes[21–26] have excellent oil/water selectivity, high sorption capacities and good recyclability. But adsorbing heavy crude oil, which is highly viscous at room temperature (more than 10^4 mPa s at 20 °C), was not demonstrated in these studies. The high viscosity of crude oil renders the adsorption extremely slow. Therefore, an effective approach to improve crude oil remediation is to lower its viscosity, which can be realized by increasing the temperature. Very recently, Joule-heating sponge and solar-heating absorbent materials that can heat the crude oil in the site have been utilized for the high-speed sorption of viscous crude oil.[27–30] Both Joule-heating and solar-heating have their own advantages. Joule-heating sponge can reach a stable temperature without being affected by the weather and the heat energy which has been transferred to crude oil can be saved for oil recovery, while photothermal materials can save operation costs.

Herein, we report a fast and all-weather MXene wrapped sponge absorbent, which can combine the advantages of *in situ* solar-heating and Joule-heating and enable fast clean-up of viscous crude-oil spills in the changeable marine environment. MXenes are one member of a family of two-dimensional (2D) transition-metal carbides or nitrides with the formula of $M_{n+1}X_nT_X$, where M represents an early transition metal, X represents carbon or nitrogen, $n = 1$, 2, or 3, T represents surface groups (–O, –OH, and/or –F), and X represents the number of the groups.[31] $Ti_3C_2T_X$, one typical member of MXenes, has outstanding metal-like conductivity of approximately 10^6 S m^{-1} and high internal light-to-heat conversion efficiency (nearly 100%).[32–37] Commercial polyurethane (PU) sponge is chosen as the porous substrate because of its low cost, good flexibility, low density, high porosity and good thermal stability. Therefore, $Ti_3C_2T_X$@PU with solar-heating and Joule-heating capabilities could significantly reduce the viscosity of heavy crude oil and

[a]School of Materials Science and Engineering, Key Laboratory of Advanced Ceramics and Machining Technology of Ministry of Education, Tianjin University, Tianjin 300072, China. E-mail: rsguo@tju.edu.cn

[b]Key Laboratory for Green Chemical Technology of Ministry of Education, State Key Laboratory of Chemical Engineering, School of Chemical Engineering and Technology, Tianjin University, Tianjin 300072, China. E-mail: junchaolao@tju.edu.cn; jluo@tju.edu.cn

[c]Key Laboratory of Materials Processing and Mold (Zhengzhou University), Ministry of Education, Zhengzhou 450002, China

[d]Physics of Complex Fluids, University of Twente, Enschede, 7500AE, The Netherlands

[e]Jiangxi Key Laboratory of Nanobiomaterials, Institute of Advanced Materials, East China Jiaotong University, Nanchang 330013, China

† Electronic supplementary information (ESI) available. See DOI: 10.1039/d0ta06480g

‡ C. G. and J. L. contributed equally to this work.

absorb the oil at a high speed at all times of the day or night (Fig. 1). It could capture 43 times its own weight of crude oil with more than 80% of oil recovery capability under the optimal conditions.

2. Results and discussion

2.1 Characterization of the $Ti_3C_2T_X$@PU sponge absorbent

To prepare the $Ti_3C_2T_X$@PU sponge absorbent, $Ti_3C_2T_X$ was first exfoliated to monolayer sheets, as revealed by transmission electron microscopy (TEM) (Fig. S1†). The $Ti_3C_2T_X$ sheets were coated on PU sponge by a multiple impregnation method (Fig. 2a and S2†).

Scanning electron microscopy (SEM) images show that the porous structure of PU still exists after coating treatment (Fig. S3†) and wrinkles are observed on $Ti_3C_2T_X$@PU. The elemental maps of carbon, fluorine and titanium indicate the uniform wrapping of $Ti_3C_2T_X$ on the PU surface (Fig. 2b). The X-ray diffraction (XRD) pattern of $Ti_3C_2T_X$@PU shows a peak at 5.7°, which demonstrates that $Ti_3C_2T_X$ has been successfully coated on the surface of the sponge fibres (Fig. S4†).

According to the FTIR spectrum shown in Fig. S5,† after loading $Ti_3C_2T_X$ on the sponge, the peak corresponding to the C–O bond undergoes a blue shift, which suggests the chemical adhesion of the MXene to PU sponge. In addition, the X-ray photoelectron spectroscopy (XPS) spectra of $Ti_3C_2T_X$ nanosheets and $Ti_3C_2T_X$@PU have been measured (Fig. S6†). As shown in the high-resolution Ti 2p of $Ti_3C_2T_X$ nanosheets (Fig. S6b†) and $Ti_3C_2T_X$@PU (Fig. S6d†), after $Ti_3C_2T_X$ coating, the Ti–O–C– bond appears on the surface of $Ti_3C_2T_X$@PU, which further proves that $Ti_3C_2T_X$ and sponge are combined through chemical bonds.[38]

As an oil absorbent, both hydrophobicity and lipophilicity are indispensable for water/oil separation. The pristine PU sponge is amphiphobic (Fig. S7†). However, the $Ti_3C_2T_X$ coating endows the PU sponge with lipophilic properties and the $Ti_3C_2T_X$@PU sponge still remains hydrophobic at the same time. As shown in Fig. 2c, $Ti_3C_2T_X$@PU exhibits contact angles of 122 ± 3° for water and 0° for vegetable oil. Hence, $Ti_3C_2T_X$@PU has an essential ability for oil/water separation *via* the coating treatment. $Ti_3C_2T_X$@PU could absorb 20–42 times its own weight in a range of organic liquids due to its inherent low density and high porosity (Fig. S8†).

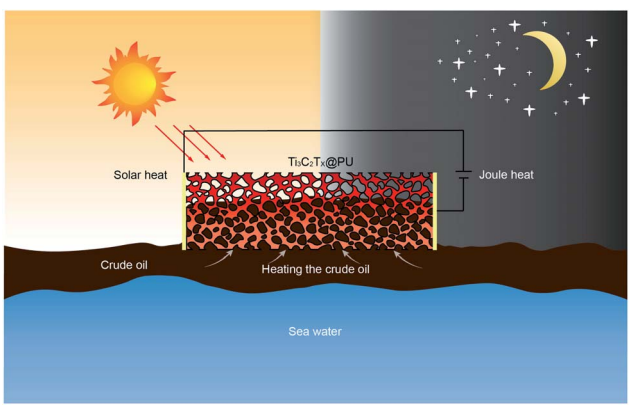

Fig. 1 Schematic illustration of all-weather $Ti_3C_2T_X$@PU used for viscous oil cleanup. $Ti_3C_2T_X$@PU can heat the crude oil to reduce the viscosity of the oil by coupling solar heat with Joule heat to achieve all-weather operation.

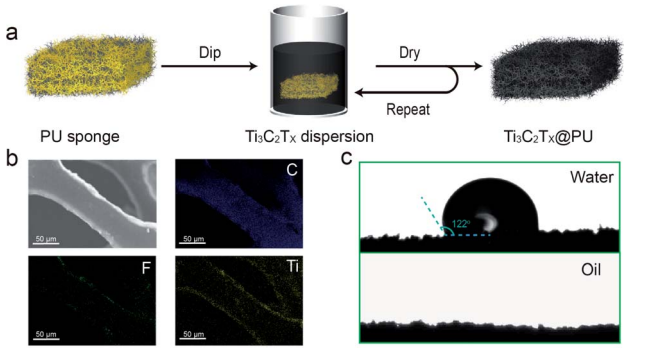

Fig. 2 Fabrication of $Ti_3C_2T_X$@PU and the characterization of the morphology. (a) Schematic illustration of the fabrication process of $Ti_3C_2T_X$@PU. (b) SEM image and corresponding C, F, and Ti elemental mapping images show the uniform $Ti_3C_2T_X$ coating on PU. (c) Surface hydrophobic and lipophilic characterization of $Ti_3C_2T_X$@PU.

2.2 Temperature dependent crude oil absorption

The rate of capillary force induced absorption is highly dependent on the viscosity of the crude oil, which can be explained theoretically by using eqn (1)[39]

$$K_S = \left[d_1\sqrt{\frac{\gamma}{\mu}}\right]\left[\sqrt{\frac{\varepsilon^*}{\lambda}}\sqrt{r_0}\right]\left[\sqrt{\frac{\cos\theta}{2}}\right] \quad (1)$$

where K_s is the liquid sorption coefficient, d_1, γ and μ are the density, surface tension and viscosity of the oil, respectively, ε^* is the effective sorption porosity of the sorbent, λ is the average tortuosity factor of the capillaries ($\lambda > 1$), r_0 is the average pore radius and θ is the contact angle of the interface between the oil and the pore wall of the sorbent. As shown in eqn (1), the absorption rate will decrease as the viscosity increases. As expected, due to its extremely high viscosity (16 740 mPa s) at room temperature, the heavy crude oil droplet (~200 μL) on the top surface of $Ti_3C_2T_X$@PU maintained its original spherical shaped surface for over 2 days at 20 °C (Fig. S9†). When the temperature of the crude oil increases, the viscosity will decrease. Indeed, we recorded the change of oil viscosity as a function of oil temperature from 20 to 120 °C (Fig. 3a), and observed that the viscosity decreases over two orders of magnitude. The reduction of viscosity leads to the increase of the liquid sorption coefficient K_s, which increases the speed of absorption significantly. When $Ti_3C_2T_X$@PU was preheated to 80 °C, the heavy crude oil droplet (~200 μL) on its top surface was also heated and completely absorbed into the sponge within 160 s (Fig. 3b). The maximum absorption capacity of $Ti_3C_2T_X$@PU at various temperatures was examined. $Ti_3C_2T_X$@PU was placed on the crude oil which had been preheated to different temperatures using a hot plate and then the absorption process proceeded. As the temperature increased

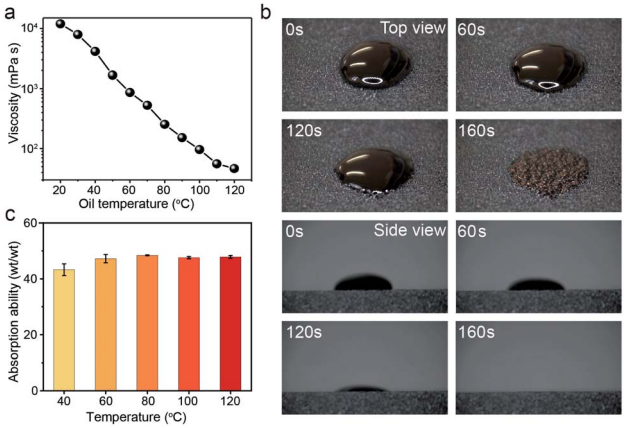

Fig. 3 Oil absorption behavior of $Ti_3C_2T_X$@PU. (a) The change of oil viscosity as a function of oil temperature. (b) Top-view and side-view images showing the oil absorption behavior of one oil droplet (~200 μL) on the surface of $Ti_3C_2T_X$@PU at 80 °C. (c) Crude oil absorption ability of $Ti_3C_2T_X$@PU at different temperatures.

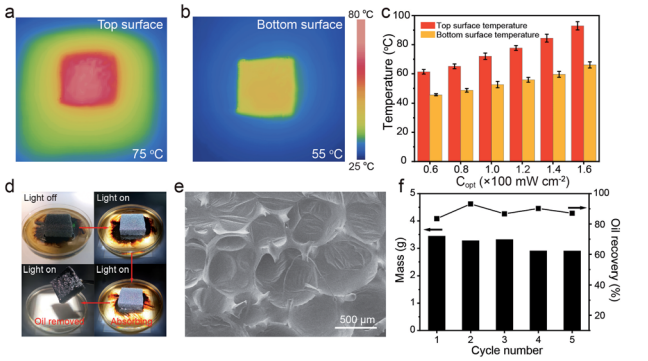

Fig. 4 Solar-assisted oil absorption by $Ti_3C_2T_X$@PU. (a and b) Infrared (IR) images of the top and bottom surfaces showing the solar-heating performance of $Ti_3C_2T_X$@PU under 1 sun solar irradiation (100 mW cm^{-2}). (c) Corresponding surface temperatures with the different solar powers. (d) Photographs showing the absorption of the crude oil on water with the aid of solar irradiation. (e) SEM images showing the microstructure of $Ti_3C_2T_X$@PU after oil absorption. (f) The mass of heavy oil absorption and the oil recovery percentage of $Ti_3C_2T_X$@PU (2 × 2 × 1 cm^3, 81.1 mg).

from 40 °C to 60 °C, the absorption ability of $Ti_3C_2T_X$@PU rose from 43 g g^{-1} to 47 g g^{-1} (Fig. 3c). This is because the high viscosity of the crude oil at a low temperature inhibits the absorption of the oil. When the temperature rises further, the absorption ability of $Ti_3C_2T_X$@PU becomes constant at a maximum of 48 g g^{-1}, which means $Ti_3C_2T_X$@PU has reached its maximum crude oil absorption capacity and higher temperature only accelerates the absorption rate.

2.3 Solar-heating assisted crude oil absorption

The solar assisted crude oil absorption by $Ti_3C_2T_X$@PU is first studied. It has been reported that $Ti_3C_2T_X$ shows broadband light absorption and has high light-to-heat conversion efficiency which was measured to be nearly 100%.[36] Absorption spectroscopy between 200 and 2500 nm shows that $Ti_3C_2T_X$@PU exhibits high absorption in the near-infrared range and the average solar absorption is 84.6% (Fig. S10†).[36,40] The photothermal effect is advantageous for reducing the viscosity of crude oil. A piece of $Ti_3C_2T_X$@PU with length × width × height of 2 × 2 × 1 cm^3 was exposed to solar irradiation of 1 sun (100 mW cm^{-2}). The temperature of the illuminated surface rises to 75 °C within 2 min and that of the bottom surface which is in contact with oil or water in the subsequent tests could reach 55 °C (Fig. 4a and b). To further demonstrate the photothermal performance, the temperatures of $Ti_3C_2T_X$@PU were measured under different light intensities. The average temperature of the bottom surface increased from 45.7 °C to 66.1 °C as the light intensities rose from 60 mW cm^{-2} to 160 mW cm^{-2} (Fig. 4c). According to the change of oil viscosity as a function of oil temperature we have found that (Fig. 3a), when the crude oil is placed at 27 °C (Fig. S11c and d†), the viscosity of crude oil is 8460 mPa s. Under 1 sun irradiation (100 mW cm^{-2}) for 10 min, the crude oil can reach the highest temperature. The average temperature of the top surface is approximately 45 °C. The temperature of the bottom surface of the crude oil with a thickness of 9 mm is 37 °C. The viscosity of crude oil is >3000 mPa s. The oil viscosity changes on its own with solar heating (without MXene) to <5460 mPa s. During an outdoor test, the solar irradiation changes constantly. The temperature response of $Ti_3C_2T_X$@PU to natural sunlight was recorded at different times of the day. The temperature of the bottom surface of the specimen is over 50 °C from 10:00 a.m. to 14:00 p.m. on August 28, 2019, in Tianjin (Fig. S12†). The results illustrate that $Ti_3C_2T_X$@PU could maintain remarkable photothermal performance in practical situations.

To demonstrate the excellent selectivity for oil absorption through photothermal effects in a site, a lab experiment was set up to simulate the practical application situation. Firstly, heavy crude oil was distributed on the water surface to make a pie-shaped oil film. A piece of $Ti_3C_2T_X$@PU was then placed on the oil film, which would float on the top because of the light weight of $Ti_3C_2T_X$@PU and the high viscosity of the crude oil. When the solar simulator was switched off, the shape of the crude oil film barely changed for a long time due to the high viscosity of the crude oil. Once irradiation begins, the area of crude oil continuously shrank, revealing that $Ti_3C_2T_X$@PU was absorbing the oil continuously (Fig. 4d). After 20 min, $Ti_3C_2T_X$@PU was lifted. There was almost no oil left on the water. SEM images obviously indicate that the inside pores of $Ti_3C_2T_X$@PU are filled with oil, which directly demonstrates the feasibility of this approach (Fig. 4e).

In addition, the recoverability of the absorbed crude oil and the cycle life of the sorbent are also critical for practical applications. In this work, $Ti_3C_2T_X$@PU was first placed on the oil under 1 sun irradiation for 20 min to let the sponge fully absorb the crude oil. After that the oil was squeezed out of $Ti_3C_2T_X$@PU by manual pressure. The same sponge was then reused for the subsequent tests. In the first cycle, $Ti_3C_2T_X$@PU absorbs 43 times its own weight (81.1 mg) of crude oil and maintains a high recovery rate (over 80%) during the first 5 cycles of oil absorption and recovery (Fig. 4f).

2.4 Joule-heating assisted crude oil absorption

Since $Ti_3C_2T_X$@PU is electrically conductive, Joule-heating can be applied to assist the crude oil absorption process without irradiation. Two pairs of graphite rods were secured to the ends of the $Ti_3C_2T_X$@PU sponge with copper wires (Fig. 5a). A 5 V stepwise increased voltage was applied on $Ti_3C_2T_X$@PU. The surface temperature increases as the voltage increased according to Joule's law (Fig. 5b). At 15 V, the temperature could reach 100 °C. The heating rate is within dozens of seconds. When the voltage rose to 20 V, the maximum surface temperature reached more than 125 °C and the resistance of $Ti_3C_2T_X$@PU began to increase significantly which indicates that the voltage at this point has already exceeded the threshold voltage of the $Ti_3C_2T_X$@PU sample with the size of 3 × 3 × 1 cm^3 (Fig. S13†). Therefore, $Ti_3C_2T_X$@PU can work below the maximum surface temperature of 120 °C. With Joule heating assistance, the crude oil was absorbed into $Ti_3C_2T_X$@PU with a maximum surface temperature of 100 °C within a few minutes (Fig. 5c). In contrast, when unpowered $Ti_3C_2T_X$@PU was brought into contact with the crude oil, the oil just adhered to the contact surface of the sponge rather than being absorbed. As the sponge was lifted, the oil attached to the surface dripped off swiftly (Fig. S14†).

2.5 Coupling solar- and Joule-heating assisted crude oil adsorption

The simultaneous solar-heating and Joule-heating features of $Ti_3C_2T_X$@PU sponge make it tolerant to weather change and harsh marine conditions in a real scenario. Accordingly, the excellent solar-heating and Joule-heating coupling effect of $Ti_3C_2T_X$@PU can make it adapt to all-weather conditions in practical use. With an indoor simulative setup, we fixed the voltage across $Ti_3C_2T_X$@PU at 10 V and then increased the light intensity gradually to measure the average surface temperature (Fig. 6a).

As shown in Fig. 6b (red spheres), when the light intensity was set at 0.6 sun, the temperature of $Ti_3C_2T_X$@PU exceeded 80 °C which was much higher than that induced by individual solar heating (0.6 sun, 61 °C) or individual Joule heating (10 V, 53 °C). When the light intensity increased to 1.6 sun, the average surface temperature of $Ti_3C_2T_X$@PU increased to 106 °C. Furthermore, when the exposed simulated solar irradiation of $Ti_3C_2T_X$@PU was set to 1 sun, the temperature of $Ti_3C_2T_X$@PU rose from 72 °C to 116 °C as the bias voltage increased from 0 V to 15 V (blue squares in Fig. 6b). The IR images correspond well to the aforementioned results (Fig. 6c). The results indicate that the temperature of $Ti_3C_2T_X$@PU can be stabilized at a higher value by coupling solar-heating and Joule-heating.

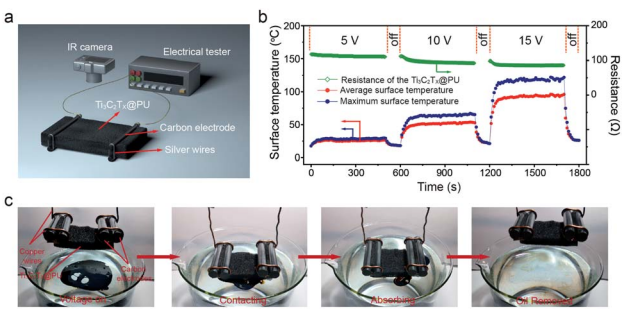

Fig. 5 The oil absorption by Joule-heating of $Ti_3C_2T_X$@PU. (a) Schematic illustration of the setup to measure the surface temperature of $Ti_3C_2T_X$@PU with different applied voltages. (b) The resistance and surface-temperature changes of $Ti_3C_2T_X$@PU (3 × 3 × 1 cm^3) with different applied voltages. Before increasing the voltage, the former voltage was turned off to bring the sponge to room temperature. (c) Photographs showing the absorbent process with the aid of Joule heating.

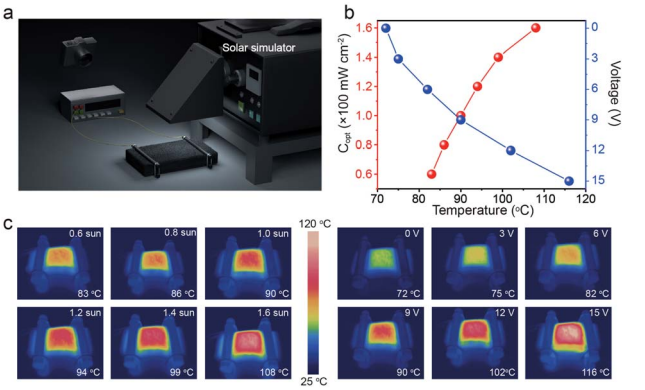

Fig. 6 Solar-heating and Joule-heating coupling properties of $Ti_3C_2T_X$@PU. (a) Schematic illustration of the setup to measure the surface temperature of $Ti_3C_2T_X$@PU with different applied voltages and solar irradiance. (b) The surface-temperature changes of $Ti_3C_2T_X$@PU applied with 10 V, different light intensities (red spheres) and 1 sun solar irradiation, and different voltages (blue squares). (c) IR images corresponding to (b). The left images correspond to the red spheres and the right one corresponds to the blue squares.

3. Conclusions

In conclusion, we demonstrate an all-weather sorbent to realize the cleanup of highly viscous crude oil spills in an efficiency manner. The high photothermal conversion efficiency and the high conductivity of $Ti_3C_2T_X$ endow the sponge absorbent with solar-heating and Joule-heating features and make it adapt to all-weather conditions in practical use. With 100 mW cm^{-2} solar irradiation, the temperature of the irradiated surface was 75 °C and the bottom surface could reach 55 °C. In the case of Joule heating, $Ti_3C_2T_X$@PU can work stably at 120 °C. This study illustrates that $Ti_3C_2T_X$@PU can achieve an appropriate temperature (nearly 120 °C) by means of the synergistic effect of solar heating and Joule heating. The viscosity of the crude oil significantly decreased to <1000 mPa s once heated, which greatly improves the efficiency of passive capillary absorption so that $Ti_3C_2T_X$@PU can capture more than 40 times its own weight of crude oil in 20 min. Remarkably, the oil absorbency of $Ti_3C_2T_X$@PU is comparable with that of other materials in many studies, as shown in Table S1.†[27–29] Moreover, the excellent coupling ability enables it to respond quickly and efficiently to oil spills under complex and volatile marine conditions. The all-

weather sorbent is expected to provide to a feasible solution for highly efficient cleanup of viscous crude oil spills.

4. Experimental section

4.1 Preparation of the $Ti_3C_2T_X$ suspension

Firstly, 0.5 g LiF and 1.3 g Ti_3AlC_2 (200 mesh, Materials Research Centre, Ukraine) were slowly added into 20 mL HCl solution. The mixture was kept at 37 °C for 24 h under vigorous stirring. After that, it was centrifugally separated at 4000 rpm. The solid residue was washed with deionized (DI) water and centrifuged again under the same conditions. This process was repeated several times until the pH value of the liquid was above 5. Finally, the washed residue was added into 120 mL of DI water, followed by ultrasonic treatment for 15 min, and centrifugal separation at 4000 rpm for 15 min. The supernatant was collected as the final suspension of $Ti_3C_2T_X$.

4.2 $Ti_3C_2T_X$ coating on PU sponge

$Ti_3C_2T_X$@PU was obtained by a dip-coating method. Commercially available PU sponge was used as a substrate. The original PU sponge was first cleaned with deionized (DI) water and ethanol successively assisted by ultrasonication. It was dried in an oven at 80 °C for 1 h. Subsequently, the cleaned sponge was dipped into the $Ti_3C_2T_X$ aqueous dispersion for 5 min, followed by drying at 80 °C for 20 min. The dipping and drying cycles were repeated four times to obtain a high loading of $Ti_3C_2T_X$ (loading ratio: 8.4 ± 0.2 wt%).

4.3 Characterization

The SEM images of the morphology and structure of original PU and $Ti_3C_2T_X$@PU were obtained with a Hitachi S-4800. The TEM image of $Ti_3C_2T_X$ nanosheets was characterized by field emission transmission electron microscopy (JEM-2100F). The contact angles of water and vegetable oil on $Ti_3C_2T_X$@PU were measured at room temperature using a contact angle system SDC-200. The viscosity of the crude oil was determined with a Physica MCR 301 rheometer. The temperature and thermal images of $Ti_3C_2T_X$@PU were obtained using a FLIR ONE infrared camera. Simulated solar radiation was created using a SAN-EI ELECTRIC XES-40S1 (wave length in the range of the standard solar spectrum AM 1.5G). The resistance of $Ti_3C_2T_X$@PU was tested using a digital galvanometer (Keithley 2400). XPS was conducted using a Physical Electronics PHI5802 instrument using a magnesium anode (mono-chromatic Kα X-ray at 253.6 eV) as the source. The binding energy in the XPS spectra was calibrated with carbon signals (C1s at 284.6 eV). XRD spectra were collected using a D8 Advanced with Cu Kα radiation.

4.4 Oil collection experiment setup

4.4.1 Absorption ability measured. In order to measure the absorption ability of $Ti_3C_2T_X$@PU at different temperatures, the crude oil was first heated to a specified temperature in an oil bath. Then a piece of $Ti_3C_2T_X$@PU ($1 \times 1 \times 1$ cm^3) was placed on the surface of the crude oil. $Ti_3C_2T_X$@PU was weighed after 5 min when it was fully filled with crude oil.

4.4.2 Solar-heating assisted oil absorption. Firstly, heavy crude oil was distributed on the water surface to make an oil film. After that, a piece of $Ti_3C_2T_X$@PU ($2 \times 2 \times 1$ cm^3) was placed on the oil film. Then the solar simulator was turned on and the light intensity was adjusted to 1 sun for solar assisted oil absorption.

4.4.3 Solar-heating assisted oil absorption cycle life measured. At first, $Ti_3C_2T_X$@PU ($2 \times 2 \times 1$ cm^3) is placed on the oil. Afterwards it is irradiated under 1 sun for 20 min to let the sponge fully absorb the crude oil. After that the oil is squeezed out. Then the above steps are repeated and the mass change of the sponge before and after oil absorption is measured to represent the cycle life of $Ti_3C_2T_X$@PU.

4.4.4 Joule-heating assisted oil absorption. To demonstrate Joule-heating assisted oil absorption, the crude oil is placed on the surface of water, firstly. Then a piece of $Ti_3C_2T_X$@PU ($4 \times 3 \times 1$ cm^3) with both ends compressed with graphited rods and connected with copper wires is powered. When the surface temperature of the sponge reaches 100 °C, it comes into contact with crude oil and absorbs the crude oil by Joule heating.

Conflicts of interest

There are no conflicts to declare.

Acknowledgements

The authors appreciate support from the National Natural Science Foundation of China (Grant No. 51872196), Natural Science Foundation of Tianjin, China (Grant No. 17JCJQJC44100), National Postdoctoral Program for Innovative Talents (No. BX20190232), China Postdoctoral Science Foundation (No. 2019M660059) and Opening Project of Key Laboratory of Materials Processing and Mold.

Notes and references

1 C. H. Peterson, S. D. Rice, J. W. Short, D. Esler, J. L. Bodkin, B. E. Ballachey and D. B. Irons, *Science*, 2003, **302**, 2086.
2 H. K. White, P. Y. Hsing, W. Cho, T. M. Shank, E. E. Cordes, A. M. Quattrini, R. K. Nelson, R. Camilli, A. W. Demopoulos, C. R. German, J. M. Brooks, H. H. Roberts, W. Shedd, C. M. Reddy and C. R. Fisher, *Proc. Natl. Acad. Sci. U. S. A.*, 2012, **109**, 20303–20308.
3 Z. Nixon, S. Zengel, M. Baker, M. Steinhoff, G. Fricano, S. Rouhani and J. Michel, *Mar. Pollut. Bull.*, 2016, **107**, 170–178.
4 E. B. Kujawinski, M. C. Kido Soule, D. L. Valentine, A. K. Boysen, K. Longnecker and M. C. Redmond, *Environ. Sci. Technol.*, 2011, **45**, 1298–1306.
5 J. Fritt-Rasmussen, J. F. Linnebjerg, M. X. Sorensen, N. L. Brogaard, F. F. Riget, P. Kristensen, G. Jomaas, D. M. Boertmann, S. Wegeberg and K. Gustavson, *Mar. Pollut. Bull.*, 2016, **109**, 446–452.

6 M. Guix, J. Orozco, M. Garcia, W. Gao, S. Sattayasamitsathit, A. Merkoci, A. Escarpa and J. Wang, *ACS Nano*, 2012, **6**, 4445–4451.
7 D. P. Prendergast and P. M. Gschwend, *J. Cleaner Prod.*, 2014, **78**, 233–242.
8 L. van Gelderen, J. Fritt-Rasmussen and G. Jomaas, *Mar. Pollut. Bull.*, 2017, **115**, 345–351.
9 Y. Dou, D. Tian, Z. Sun, Q. Liu, N. Zhang, J. H. Kim, L. Jiang and S. X. Dou, *ACS Nano*, 2017, **11**, 2477–2485.
10 H. Sun, Z. Xu and C. Gao, *Adv. Mater.*, 2013, **25**, 2554–2560.
11 C. Wu, X. Huang, X. Wu, R. Qian and P. Jiang, *Adv. Mater.*, 2013, **25**, 5658–5662.
12 Z. Y. Wu, C. Li, H. W. Liang, Y. N. Zhang, X. Wang, J. F. Chen and S. H. Yu, *Sci. Rep.*, 2014, **4**, 4079.
13 G. Hayase, K. Kanamori, M. Fukuchi, H. Kaji and K. Nakanishi, *Angew. Chem., Int. Ed.*, 2013, **52**, 1986–1989.
14 C. Ruan, K. Ai, X. Li and L. Lu, *Angew. Chem., Int. Ed.*, 2014, **53**, 5556–5560.
15 D. D. Nguyen, N. H. Tai, S. B. Lee and W.-S. Kuo, *Energy Environ. Sci.*, 2012, **5**, 7908–7912.
16 Z. Xue, Y. Cao, N. Liu, L. Feng and L. Jiang, *J. Mater. Chem. A*, 2014, **2**, 2445–2460.
17 H. Sun, A. Li, Z. Zhu, W. Liang, X. Zhao, P. La and W. Deng, *ChemSusChem*, 2013, **6**, 1057–1062.
18 V. Chabot, D. Higgins, A. Yu, X. Xiao, Z. Chen and J. Zhang, *Energy Environ. Sci.*, 2014, **7**, 1564–1596.
19 X. Zhang, Z. Li, K. Liu and L. Jiang, *Adv. Funct. Mater.*, 2013, **23**, 2881–2886.
20 A. Li, H. X. Sun, D. Z. Tan, W. J. Fan, S. H. Wen, X. J. Qing, G. X. Li, S. Y. Li and W. Q. Deng, *Energy Environ. Sci.*, 2011, **4**, 2062–2065.
21 J. Ge, H. Y. Zhao, H. W. Zhu, J. Huang, L. A. Shi and S. H. Yu, *Adv. Mater.*, 2016, **28**, 10459–10490.
22 Z. Xue, S. Wang, L. Lin, L. Chen, M. Liu, L. Feng and L. Jiang, *Adv. Mater.*, 2011, **23**, 4270–4273.
23 S. J. Gao, Z. Shi, W. B. Zhang, F. Zhang and J. Jin, *ACS Nano*, 2014, **8**, 6344–6352.
24 C. Gao, Z. Sun, K. Li, Y. Chen, Y. Cao, S. Zhang and L. Feng, *Energy Environ. Sci.*, 2013, **6**, 1147–1151.
25 X. Y. Wang, M. J. Li, Y. Q. Shen, H. Feng and J. Li, *Green Chem.*, 2019, **21**, 3190–3199.
26 G. G. Shi, Y. Q. Shen, P. Mu, Q. T. Wang, Y. X. Yang, S. Y. Ma and J. Li, *Green Chem.*, 2020, **22**, 1345–1352.
27 J. Ge, L. A. Shi, Y. C. Wang, H. Y. Zhao, H. B. Yao, Y. B. Zhu, Y. Zhang, H. W. Zhu, H. A. Wu and S. H. Yu, *Nat. Nanotechnol.*, 2017, **12**, 434–440.
28 Y. Kuang, C. Chen, G. Chen, Y. Pei, G. Pastel, C. Jia, J. Song, R. Mi, B. Yang, S. Das and L. Hu, *Adv. Funct. Mater.*, 2019, **29**, 1900162.
29 J. Chang, Y. Shi, M. Wu, R. Li, L. Shi, Y. Jin, W. Qing, C. Tang and P. Wang, *J. Mater. Chem. A*, 2018, **6**, 9192–9199.
30 C. Zhang, M. B. Wu, B. H. Wu, J. Yang and Z. K. Xu, *J. Mater. Chem. A*, 2018, **6**, 8880–8885.
31 M. Naguib, M. Kurtoglu, V. Presser, J. Lu, J. Niu, M. Heon, L. Hultman, Y. Gogotsi and M. W. Barsoum, *Adv. Mater.*, 2011, **23**, 4248–4253.
32 X. Zhang, R. Lv, A. Wang, W. Guo, X. Liu and J. Luo, *Angew. Chem., Int. Ed.*, 2018, **57**, 15028–15033.
33 Z. Liu, R. Guo, M. Zheng, F. Li, Y. Bao, T. Li and Y. Luo, *Ceram. Int.*, 2018, **44**, 11757–11764.
34 Z. Liu, R. Guo, F. Li, M. Zheng, B. Wang, T. Li, Y. Luo and L. Meng, *J. Alloys Compd.*, 2018, **762**, 643–652.
35 J. Lao, R. Lv, J. Gao, A. Wang, J. Wu and J. Luo, *ACS Nano*, 2018, **12**, 12464–12471.
36 R. Li, L. Zhang, L. Shi and P. Wang, *ACS Nano*, 2017, **11**, 3752–3759.
37 T. H. Park, S. Yu, M. Koo, H. Kim, E. H. Kim, J. E. Park, B. Ok, B. Kim, S. H. Noh, C. Park, E. Kim, C. M. Koo and C. Park, *ACS Nano*, 2019, **13**, 6835–6844.
38 Y. M. Wu and R. M. Nix, *J. Mater. Chem.*, 1994, **4**, 1403–1407.
39 V. Beltran, A. Escardino, C. Feliu and M. D. Rodrigo, *Br. Ceram. Trans.*, 1988, **87**, 64–69.
40 K. Li, T. Chang, Z. Li, H. Yang, F. Fu, T. Li, J. S. Ho and P. Chen, *Adv. Energy Mater.*, 2019, **9**, 1901687.